



HAL
open science

A micro-transducer matrix design for the detection of flexural guided waves

Hala El Rammouz, Farouk Benmeddour, Jamal Assaad, Emmanuel Moulin, Nikolay Smagin, Lucie Dupont, Lynda Chehami, Youssef Zaatari, Ziad Herro

► **To cite this version:**

Hala El Rammouz, Farouk Benmeddour, Jamal Assaad, Emmanuel Moulin, Nikolay Smagin, et al..
A micro-transducer matrix design for the detection of flexural guided waves. *Ultrasonics*, 2021, 115, pp.106430. 10.1016/j.ultras.2021.106430 . hal-03542162

HAL Id: hal-03542162

<https://hal.science/hal-03542162v1>

Submitted on 9 May 2023

HAL is a multi-disciplinary open access archive for the deposit and dissemination of scientific research documents, whether they are published or not. The documents may come from teaching and research institutions in France or abroad, or from public or private research centers.

L'archive ouverte pluridisciplinaire **HAL**, est destinée au dépôt et à la diffusion de documents scientifiques de niveau recherche, publiés ou non, émanant des établissements d'enseignement et de recherche français ou étrangers, des laboratoires publics ou privés.



Distributed under a Creative Commons Attribution - NonCommercial 4.0 International License

A micro-transducer matrix design for the detection of flexural guided waves^{*,**}

H. El Rammouz^{a,*}, F. Benmeddour^a, J. Assaad^a, E. Moulin^a, N. Smagin^a, L. Dupont^a,
L. Chehami^a, Y. Zaatari^b and Z. Herro^b

^aUniv. Polytechnique Hauts-de-France, CNRS, Univ. Lille, ISEN, Centrale Lille, UMR 8520 - IEMN - Institut d'électronique de Microélectronique et de Nanotechnologie, DOAE - Département d'Opto-Acousto-electronique, F-59313 Valenciennes, France

^bLebanese University, Faculty of Sciences II, Laboratory of Applied Physics, Fanar, Lebanon

ARTICLE INFO

Keywords:

Micro-transducer matrix
Flexural modes
Structural health monitoring
Non-destructive evaluation

ABSTRACT

In this paper, a new approach is proposed for the detection of ultrasonic guided waves using a LiNbO₃ single crystal-based micro-transducer matrix. This matrix was designed, manufactured, and then used to detect Lamb and Pochhammer-Chree guided waves in plate- and cylinder-like structures. This study highlights the identification of the first flexural mode F(1,1) in cylinders at low frequencies. A network analyser and a laser Doppler vibrometer (LDV) were used to characterise and study the behaviour of the micro-transducer matrix. An experimental device was designed and used to acquire electrical measurements of the micro-transducer vibrations. Then, an original experimental device was developed to generate a selected flexural guided mode in a solid aluminium cylinder. The emitter comprised two semicircular piezoelectric transducers excited with only one phased signal thanks to the inverse position of polarisation. Finally, the results prove that the flexural mode F(1,1) is selected and generated by the emitter, then detected and identified by the micro-transducer matrix.

1. Introduction

Ultrasonic guided waves (UGW) have shown great potential for non-destructive evaluation (NDE) and structural health monitoring (SHM) of planar and cylindrical-like structures [1]. These waves can propagate over long distances in metallic structures without being significantly attenuated. However, due to the dispersive and multi-modal nature of these waves, the physical interpretation of their interactions with any damage is complex. It is therefore necessary to study the propagation of a single mode to simplify the analysis of the structural inspection.

The interaction of a single guided mode with damage in plates has been the subject of several numerical and experimental studies [2, 3, 4, 5]. Regarding cylindrical structures, research has been primarily carried out on pipes and tubes. UGW in these structures are also known as Pochhammer-Chree modes [6]. Lowe et al. [7] proposed a method for selecting the longitudinal mode L(0,2) in a pipe and studied its interaction with defects of different dimensions. Djili et al. [8] investigated the detection of "notch" type defects in tubes immersed in water using the same mode. Demma et al. [9] exploited the torsional mode T(0,1) for the NDE of pipes. Finally, the review paper [10] summarises the use of compressional waves in NDE, particularly the L(0,1) and L(0,2) modes as well as the torsional mode T(0,1). Benmeddour et al. [11] carried out numerical studies on elastic cylinders to predict the scattering of the three fundamental modes L(0,1), T(0,1) and more particularly the flexural mode F(1,1) after interaction with different types of inhomogeneities. The advantage of the F(1,1) mode is that it can be launched as a "rotating" mode so different kinds of damage can be detected.

To generate and receive a single mode in a cylindrical structure, transducer network configurations have been developed [12]. For example, Zhang et al. [13] studied the preferential detection of a single longitudinal or torsional mode in hollow cylinders through the excitation of a network of transducers, with phase-shifted signals, placed around the circumference. Lowe et al. [14] presented a method for generating the L(0,1) mode using a transducer network. SHM requirements in terms of miniaturisation and integration have pushed researchers to design micron-scale transducer networks and matrices based on the deposition of thin films of piezoelectric materials [15, 16]. However, this type of manufacturing is complicated due to various challenges regarding the performance of the material deposited [15].

*Corresponding author

✉ halarammouz@gmail.com (H.E. Rammouz)

ORCID(s):

Generally, the piezoelectric material lead zirconate titanate (PZT) is used to manufacture transducers. Unfortunately, current legislation prohibits the use of lead in the microelectronics industry [17]. To this end, research has focused on the synthesis of new lead-free materials or the use of well known crystals. One of these crystals is Lithium Niobate (LiNbO_3) which has interesting electrical and mechanical properties [18, 19].

In this paper, a new approach is proposed to detect the UGW using a micro-transducer (μT) matrix based on LiNbO_3 single crystal. This matrix, having a small size and a small thickness, can be easily integrated into a structure, particularly cylindrical-like structures, for SHM applications. This matrix is used as an UGW receiver in the low frequency range [60 - 120] kHz despite its small dimensions.

To this end, section 2 presents the design of a μT matrix as well as the manufacturing process on a LiNbO_3 substrate. The process comprised four main steps: metallisation of the lower face, photolithography, metallisation, and lift-off of the upper face. Several matrices 500.44 μm thick were obtained. These were characterised using a network analyser and used in this research work.

Section 3 deals firstly with the detection of Lamb waves in an aluminium plate. Normal displacement measurements were acquired using LDV to verify the behaviour of the matrix in relation to the propagation of guided waves. Secondly, LDV measurements were carried out on a solid aluminium cylinder to show the ability of the matrix to detect and separate the mode shapes of Pochhammer-Chree waves.

The selection and generation of the F(1,1) mode between 60 kHz and 120 kHz using an actuator comprising two piezoelectric half-pads are presented in section 4. Electrical measurements were conducted on the matrix elements to demonstrate the detection of this mode using the μT matrix.

2. Development and characterisation of an acoustical micro-transducer matrix

In this section, the design and the manufacturing process of the LiNbO_3 -based μT matrix is presented. A LiNbO_3 single crystal 36° Y-cut (rotation 36° around the Y axis) substrate 76 mm in diameter and 500 μm thick was used. This cut was chosen for its attractive properties and its sensitivity to surface waves [20].

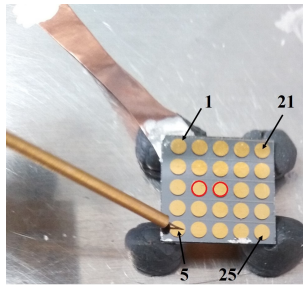


Figure 1: Photograph of a μT matrix.

A matrix is made up of 25 circular μT s (see Figure 1). Each μT has a diameter equal to 1.5 mm. The center-to-center spacing of two consecutive μT s is 2 mm. The matrix was initially designed to fit a cylinder cross-section of 14 mm in diameter and since the measurements are done manually, a maximum number of 25 μT is chosen to reduce the time it takes to acquire data, and also so that the test probes used for the electrical measurements can fit accurately the μT s.

The manufacturing process was based on two main techniques: metallisation and photolithography, performed on the LiNbO_3 piezoelectric substrate. This process was chosen, on the one hand, to avoid the deposition of the piezoelectric material which is challenging, time-consuming, and expensive. On the other hand, the metallisation technique is well known and the photolithography allows to define the matrix pattern.

The manufacture of this matrix involved several steps. First, the joint electrode (the earth electrode) of all the μT s was deposited by metallising a face of the substrate with a 200 nm layer of gold. A 20 nm gripping layer of chromium was deposited between the wafer and the gold (see Figure 2a). The remaining steps were performed on the non-metallised substrate face. First, the surface was conditioned. Thermal annealing at 110°C for 5 minutes was applied to ensure

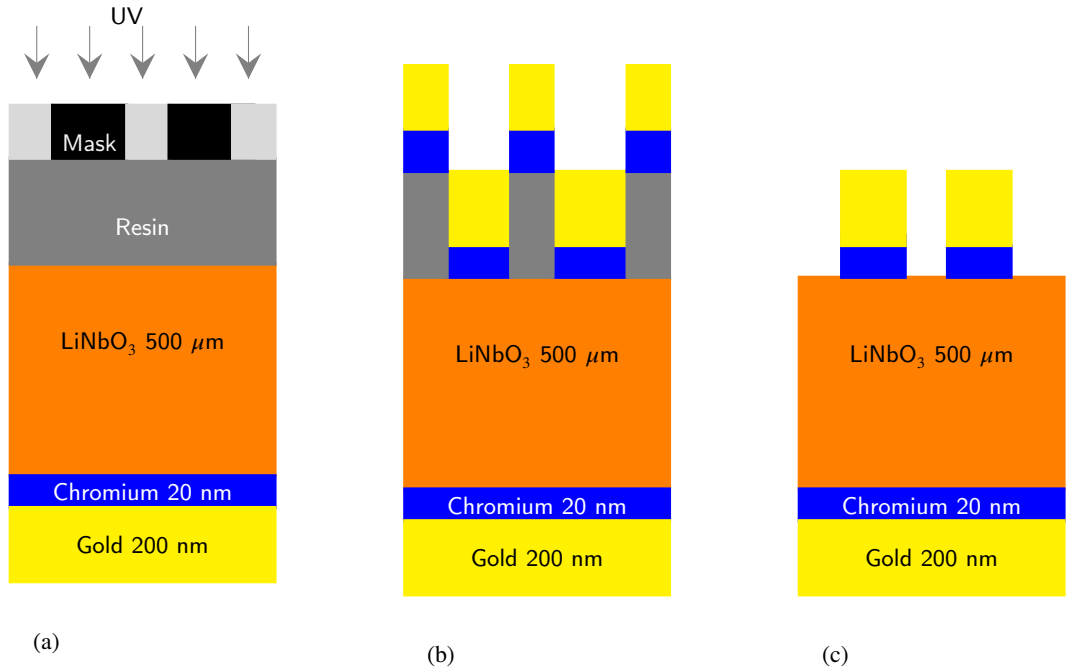


Figure 2: Manufacturing procedure a) Joint electrode deposition and photolithography, (b) Resin development and deposition of the upper electrodes, (c) Lift-off .

dehydration of the surface. Then, an HMDS-type (hexamethyldisilazane) chemical solution was used to clean the surface. The latter was deposited using spin-coating to improve the adhesion of the resin. After surface conditioning, a layer of AZ nLOF2020-type negative resin approximately $2 \mu\text{m}$ thick was deposited using spin-coating (see Figure 2a). The deposition was immediately followed by thermal annealing at 110°C for 90 s to reinforce the bonds between the resin molecules and then exposure to 'hard' ultraviolet radiation for 7 s. Thereafter, thermal annealing at 110°C for 90 s was applied to amplify the development and reinforce the bonds in the exposed photoresist. Then, the resin was developed by immersing the substrate in a basic A326-type solution for 90 s (see Figure 2b). Regarding the upper electrodes, a 20 nm chromium layer and a 200 nm gold layer were deposited successively (see Figure 2b). Finally, the resin layer and the metal deposited were removed during surface "lift-off" (see Figure 2c). This was achieved by immersing the substrate for a few hours in an SVC-175-type remover solvent heated to 65°C .

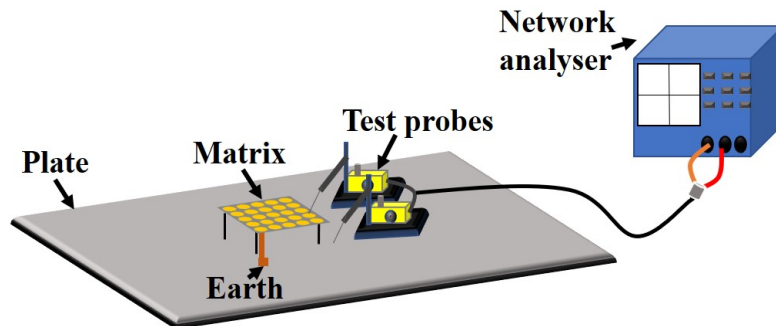


Figure 3: Experimental setup to measure the μT s electrical impedance

Figure 3 depicts the experimental setup to characterise the μT s. It consists of a Wayner Kerr 6540A network

analyser connected to Quarter A-20338 test probes. One probe is connected to a μT in the matrix, while the other is connected to the earth. The matrix is supposed to be free from any mechanical load (Figure 1). The voltage applied across the μT was 1 V. A frequency sweep from 1 kHz to 15 MHz was performed on two μT s in the centre: μT numbers 8 and 13 (μT s marked in red in Figure 1) to determine their resonant frequencies. The measurements were then carried out on the 25 μT s in the matrix around the resonance frequency (between 7.0 MHz and 7.6 MHz).

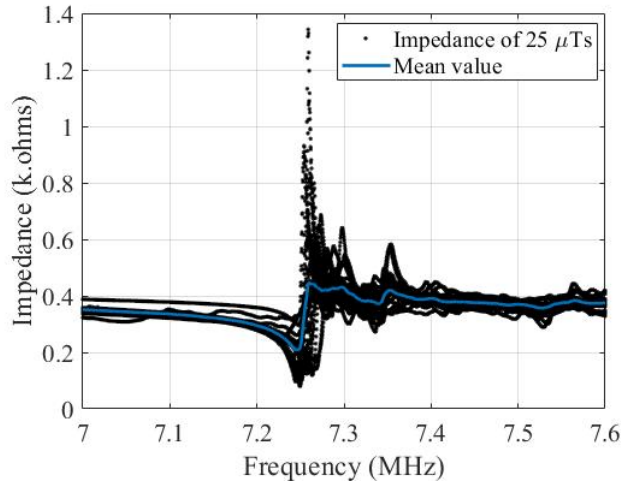


Figure 4: Electrical impedance versus frequency for the 25 μT s.

Figure 4 shows the variation in the electrical impedance as a function of the frequency for the 25 μT s in the matrix 500,44 μm thick. The continuous blue curve represents the average impedance. Good reproducibility was observed for the 25 μT s. In the following, the ability of the matrix to operate in the low frequency range was demonstrated despite its high resonance frequency.

3. Identification of guided waves using the micro-transducer matrix

3.1. Identification of Lamb modes

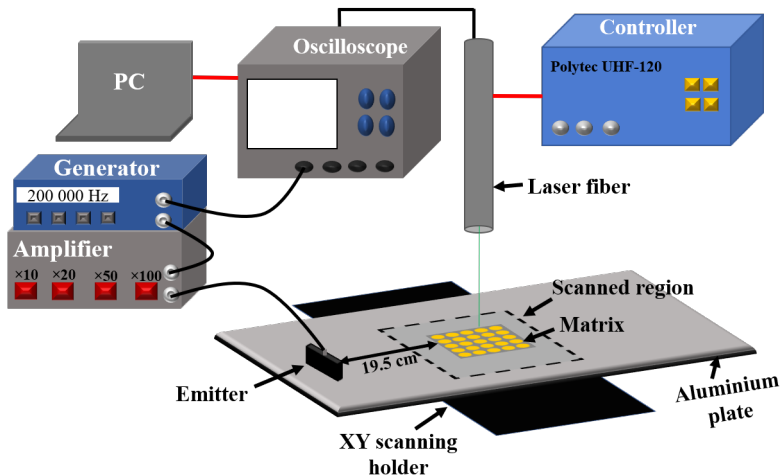


Figure 5: Experimental setup to visualise the propagation of Lamb waves in an aluminium plate.

In the experimental setup in Figure 5, the μT matrix was placed on an aluminium plate ($500 \times 150 \times 6 \text{ mm}^3$) at a distance of 19.5 cm from the emitter. To ensure good coupling, a thin layer of petroleum grease was used. The plate was placed on the XY scanning support. The UGW were excited using a Panametrics A413S 0.5/0.5X1.0 transducer. The excitation signal was a tone burst with 7 cycles, a frequency of 200 kHz, and a peak-to-peak amplitude of 10 V applied by a Tektronix 7051 generator. The signals received at each measurement point are acquired using the LDV photodiode and visualised on a LeCroy 725Zi-A oscilloscope. The signals were then transmitted to a computer (PC). The region inspected by the laser includes the matrix and part of the surrounding plate. The signals were acquired at 1963 points with a spatial resolution defined by $\Delta x \times \Delta y = 0.5 \times 0.5 \text{ mm}^2$.

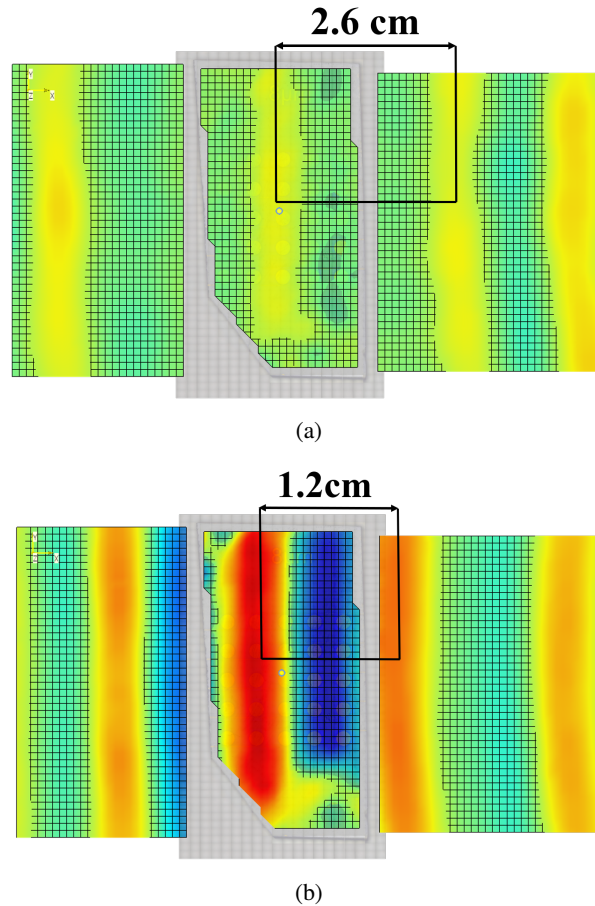


Figure 6: Visualisation of Lamb mode propagation on an aluminum plate through the matrix (a) S_0 at $t = 40 \mu\text{s}$ and (b) A_0 at $t = 60 \mu\text{s}$.

The propagation of the fundamental zero-order, symmetrical (S_0) and anti-symmetrical (A_0) Lamb modes at 40 s and 60 s are shown in Figures 6a and 6b, respectively. These were identified by measuring their wavelengths, which correspond to 2.6 cm and 1.2 cm, respectively. The absence of the reflected wave out-of-plane component with the μT matrix should be noted. Indeed, the small thickness of the μT s makes them almost transparent to the guided waves. It should be noted that the gray frames that appear in Figures 6a and 6b are due to the acquisition data system, Polytec PSV 9.2, of the LDV. In fact, the laser scanning head is coupled to a microscope and so the microscopic image of the μT matrix was combined with the acquired displacement data.

The experimental setup in Figure 5 was used again to acquire electrical measurements. These signals were then

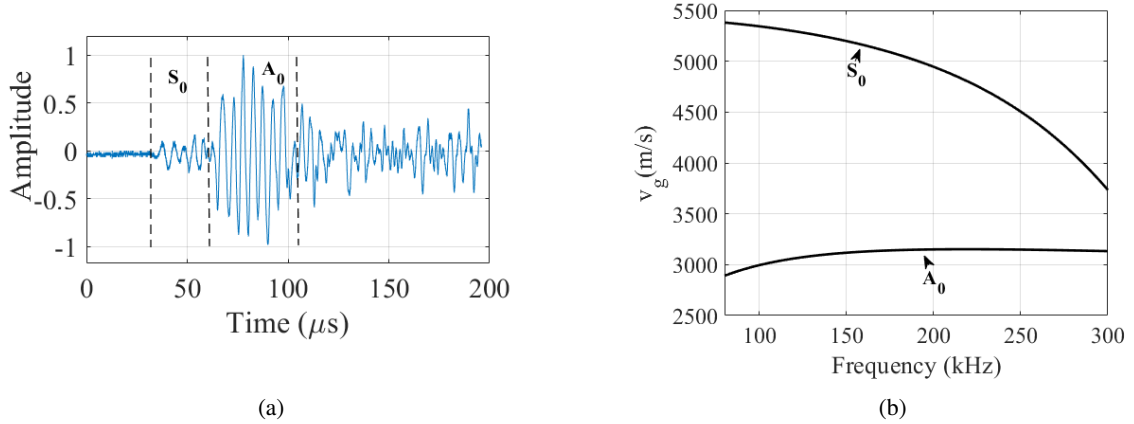


Figure 7: (a) Electrical signal acquired on a μT and (b) Dispersion curves of group velocity versus frequency in a 6 mm thick plate [21].

measured on the 25 μT s using Quarter A-20338 test probes. The result for a central excitation frequency of $f_c = 200$ kHz is shown in Figure 7a. The propagation of S_0 and A_0 modes were identified at different moments and were based on the calculation of the times of flight, noted t , for the two modes using $t = D/v_g$ where D is the distance between the emitter and the matrix and v_g is the theoretical group celerity of the S_0 and A_0 modes at 200 kHz (see Figure 7b). The times of flight obtained were 39 μs and 60 μs for the S_0 and A_0 modes, respectively. These correspond to the arrival times of the modes displayed in Figure 7a. These results show the ability of the μT s to recover the vibration of guided waves at low frequencies despite their small dimensions.

3.2. Identification of Pochhammer-Chree modes

This section aims to identify Pochhammer-Chree waves in a solid aluminium cylinder 1 m long and 14 mm in diameter. The propagation of these waves in such structures can be predicted theoretically using different numerical methods. In this study, the semi-analytical discontinuous Galerkin finite element method (SAFE-DG) [21] was used.

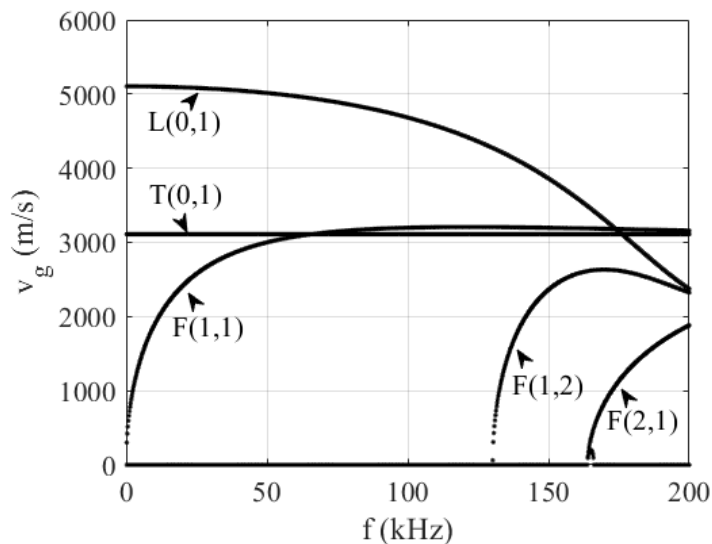


Figure 8: Dispersion curves of group velocity versus frequency [21].

Figure 8 shows the group velocity (v_g) versus frequency dispersion curves obtained with the SAFE-DG method.

Three fundamental modes were observed: T(0,1), which is a non-dispersive torsional mode as its v_g is constant; the first flexural mode, F(1,1), for which v_g is equal to zero for $f = 0$ kHz; the first compressional mode, L(0,1), which tends towards a non-zero value and is initially the fastest. As the frequency increases, the dispersion curves become more complex and several compressional and flexural modes of higher order appear.

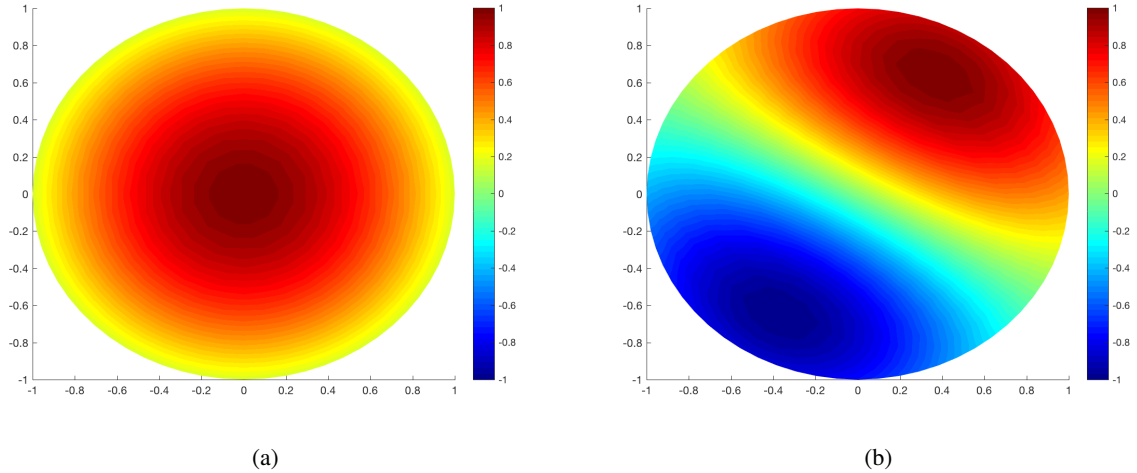


Figure 9: Mode shapes of (a) L(0,1) and (b) F(1,1) in a solid aluminium cylinder 1 m long and 14 mm in diameter for $f = 100$ kHz.

The theoretical mode shapes of the L(0,1) and F(1,1) modes are shown in Figure 9a and Figure 9b, respectively. In these figures, the colour scale represents the amplitude of the mode shapes. Figure 9a shows the symmetrical vibration of the L(0,1) mode for an $f = 100$ kHz. From this figure, one can see that the central part of the mode shape is uniform (red part in figure 9a) whereas for high frequencies more ripples will be seen [22]. Conversely, Figure 9b highlights the anti-symmetrical vibration of the F(1,1) mode.

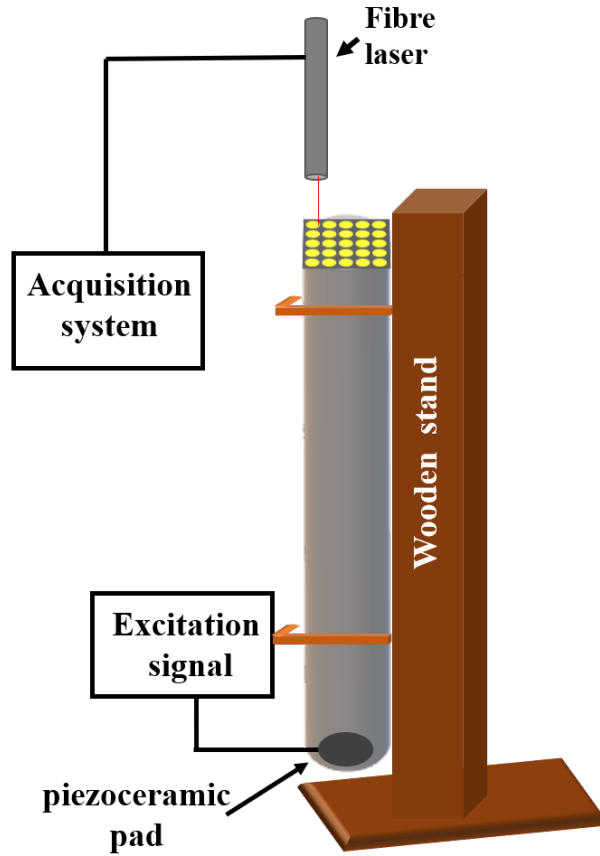
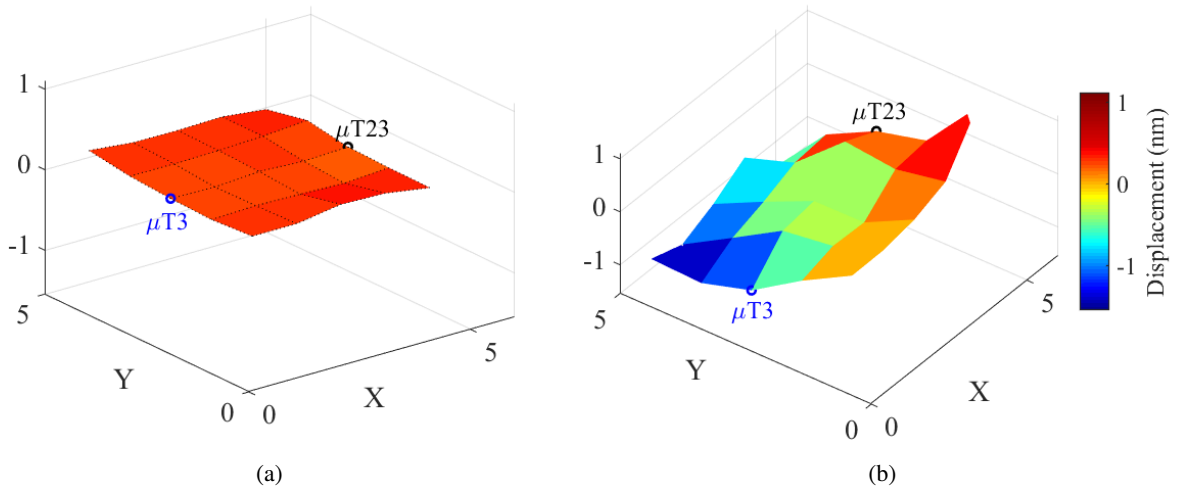
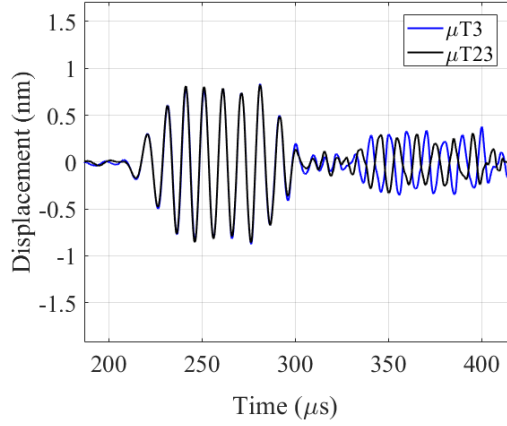


Figure 10: Experimental setup for the LDV measurements.



In the experimental setup in Figure 10, an aluminium cylinder of length $L = 1$ m and cross section of diameter $d = 14$ mm is fixed to a wooden stand. A piezoceramic transducer was used to generate UGW. The latter was excited by a tone burst of 7 cycles and a peak-to-peak amplitude of 25 V using an Agilent 33250A generator and amplified using an NF 4055 amplifier. The frequencies transmitted varied from [20 - 200] kHz with an increment of 2 kHz. The spatial



(c)

Figure 11: Mode shapes detected by LDV on the matrix at two different instants for $f_c = 100$ kHz (a) $L(0,1)$ at $t = 250$ μs , (b) $F(1,1)$ at $t = 360$ μs and (c) Signals acquired at two opposite measurement points on the matrix.

movement of the laser probe was ensured using a Newport ESP301 motion controller. A 500 μm thick matrix of 25 μT s 1.5 mm in diameter was fixed to the cylinder cross section using cyanoacrylate glue. The normal displacement of the vibration was measured on each μT . Signals were visualised on a LeCroy 64Xi oscilloscope and recorded and processed on a computer (PC).

Figures 11a and 11b show the normal displacement measured on the 25 μT s of the matrix at 250 μs and 360 μs . The X and Y axes represent the μT number in the spatial coordinate system (5×5 measurement points represented by the surface nodes, see Figure 11a). The colour intensity shows the variation in the normal displacement amplitude measured on each μT . The maximum amplitude measured is around 0.6 nm. Figure 11a depicts a flat surface corresponding to the first compressional mode $L(0,1)$. Figure 11b presents an anti-symmetrical vibration corresponding to the first flexural mode $F(1,1)$. The signals acquired at $\mu\text{T}3$ and $\mu\text{T}23$ are shown in Figure 11c. The first wave packets arriving at $t = 212$ μs at $\mu\text{T}3$ and $\mu\text{T}23$ correspond to the $L(0,1)$ mode. These wave packets are in phase, which is consistent with the expected distribution of the displacement field associated with the $L(0,1)$ mode. Conversely, the second wave packets arriving at $t = 320$ μs at $\mu\text{T}3$ and $\mu\text{T}23$ correspond to the $F(1,1)$ mode. These wave packets are in anti-phase, which is consistent with the expected distribution of the displacement field associated with the $F(1,1)$ mode.

4. Generation and identification of the $F(1,1)$ mode

In this section, a method is proposed to select and generate the $F(1,1)$ mode in an aluminium cylinder based on the anti-phased excitation of two piezoceramic semicircular transducers bound separately to the cylinder cross section. First, LDV measurements were carried out on the upper cylinder cross section. Then, electrical signals were acquired on each μT of the matrix to show the ability of the matrix to detect and identify the selected $F(1,1)$ mode.

4.1. Generation of the $F(1,1)$ mode

A Pz27 circular piezoceramic transducer 2 mm thick and 12.7 mm in diameter was cut in half (Figure 12a). The two half-transducers were then bound separately to the cylinder cross section (Figure 12b). One of the half-transducers was fixed inversely to its direction of polarisation. Hence, the two half-transducers could be excited by one phased signal with a single generator. The experimental setup in figure 10 was again used but in this case the LDV measurements were done on the empty cylinder cross section. A spatial scan was performed at 324 measurement points on the cylinder cross section with a spatial step of 800 μm . The frequency transmitted varied from $[50 - 130]$ kHz with an increment of 2 kHz.

Figures 13a and 13b show the mode shapes of $L(0,1)$ and $F(1,1)$ modes propagating in the cylinder for an f_c of 60

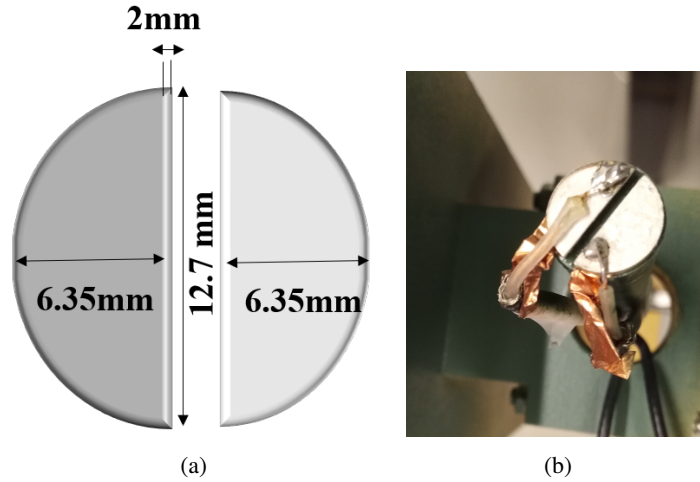


Figure 12: Emitter made of two semicircular piezoceramic transducers bound separately to the cylinder cross section (a) Diagram and (b) Photograph.

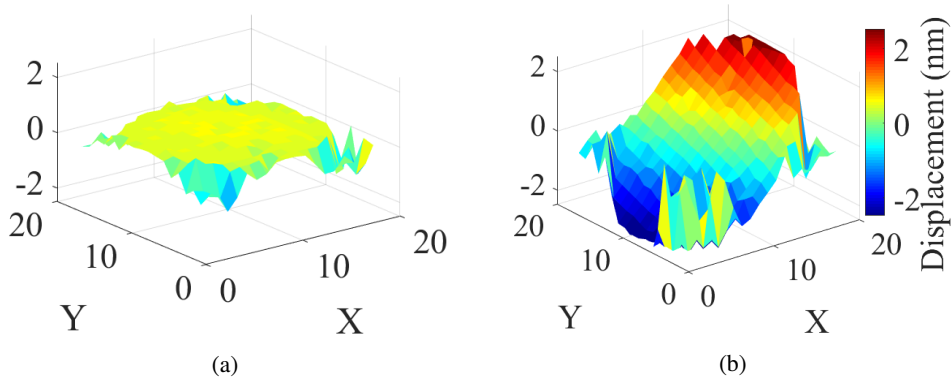


Figure 13: Mode shapes of (a) L(0,1) mode and (b) F(1,1) mode ($f_c = 60$ kHz).

kHz. These mode shapes show that the normal displacement amplitude of the L(0,1) mode is small whereas the F(1,1) mode has a relatively large amplitude of around 2 nm.

Figure 14a shows a comparison between the signals measured using LDV with two different emitters: a circular piezoceramic pad and two semicircular pads. This shows a slight normal displacement component of the L(0,1) mode arriving at $t = 212 \mu\text{s}$ using the two half-pads. Figure 14b shows the signals acquired for the different emitters for an f_c equal to 120 kHz. In Figure 14b, one can see that the amplitude of the normal displacement of the F(1,1) mode has increased. Concerning the L(0,1) mode, its out-of-plane component is detected but remains weak in comparison with that of the F(1,1) mode.

The use of an emitter made up of two semicircular piezoceramic transducers excited with one phased signal corresponding to two anti-phased signals, allows the selection and generation of the fundamental flexural mode F(1,1) in the low frequency range, particularly in the interval [60 - 120] kHz. It should be noted that a small out-of-plane component of the L(0,1) mode is detected with a maximum amplitude of 0.6 nm. On the contrary, the out-of-plane component of the F(1,1) mode varied between 2 nm and 7 nm depending on the frequency f_c .

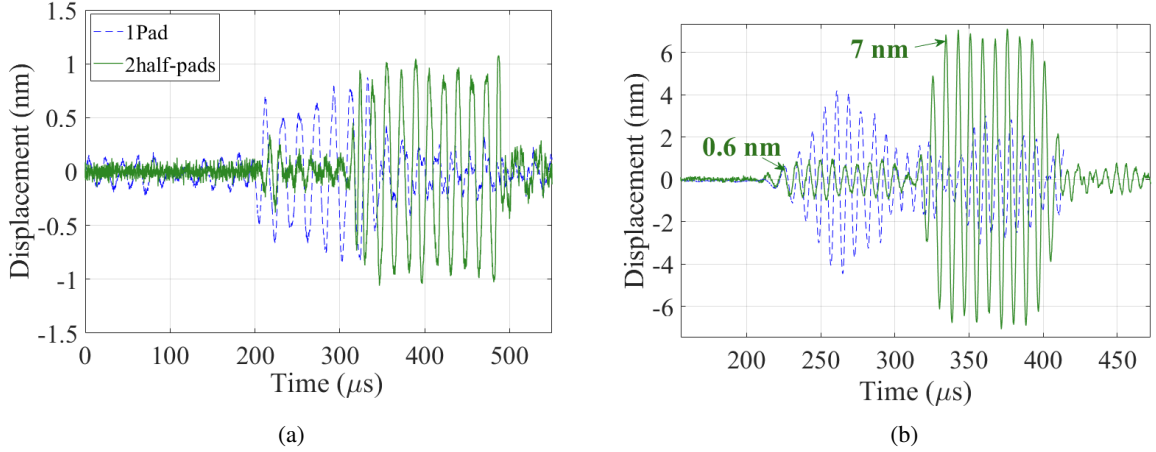


Figure 14: Measured signals by LDV using two different emitters at (a) $f_c = 60$ kHz and (b) $f_c = 120$ kHz.

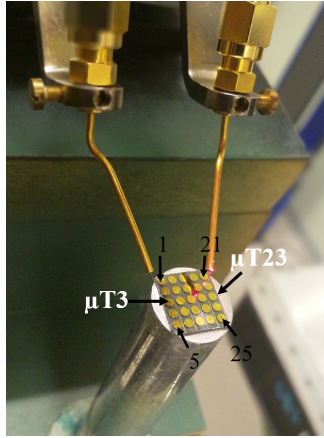


Figure 15: Photograph of the μ T matrix fixed to the cylinder cross section.

4.2. Identification of the F(1,1) mode using a micro-transducer matrix

To identify the mode shapes of the F(1,1) mode, electrical measurements were performed on the 25 μ Ts. The μ T matrix was bound to the cylinder cross section, as shown in Figure 15, by applying a thin layer of cyanoacrylate glue. The experimental setup described in section 3.2 was used. The excitation signal applied across the emitter was a tone burst of 10 cycles windowed by Hanning window with a peak-to-peak amplitude of 15 V. The frequency studied varied from [50 - 130] kHz with a 2 kHz increment. Electrical signals were measured using Quarter XYZ 300 TL test probes.

Figure 16 shows the mode shape of the F(1,1) mode at $t = 342 \mu\text{s}$ obtained with the electrical measurements. The X and Y axes represent the μ T number in the spatial coordinate system (5×5 measurement points, see figure 15). The colour intensity shows the variation in the amplitude measured on each μ T. The anti-symmetrical vibration of the F(1,1) mode with respect to a median plane of the cylinder cross section was observed. By exploiting two opposite μ Ts, one can see that μ T3 and μ T23 have opposite voltage values.

Figure 17 shows that the only mode detected by μ T3 and μ T23 was F(1,1) at $t = 316 \mu\text{s}$ at $f_c = 60$ kHz. These two signals are anti-phased between $300 \mu\text{s}$ and $500 \mu\text{s}$, which confirms the detection of the F(1,1) mode and highlights its anti-symmetrical vibration. Finally, these results prove that the flexural mode F(1,1) is selected, generated, and detected by the matrix for an $f_c = 60$ kHz.

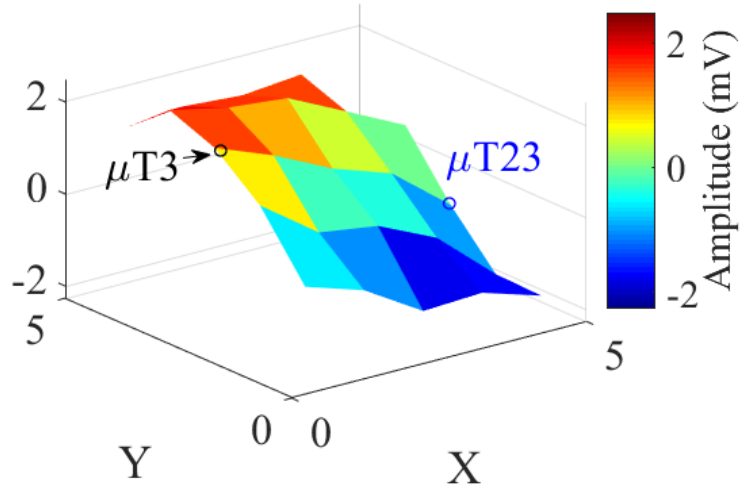


Figure 16: F(1,1) mode shapes obtained with electrical measurements for $f_c = 60$ kHz at $342 \mu\text{s}$.

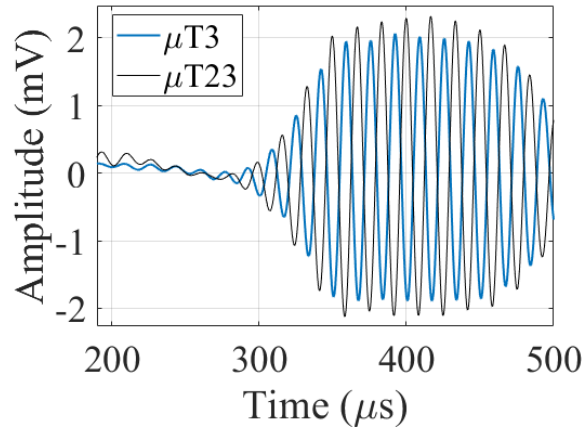


Figure 17: Electrical signals measured on μT3 and μT23 for $f_c = 60$ kHz .

5. Conclusion

In this work, a μT matrix model based on $500 \mu\text{m}$ thick 36° Y-cut LiNbO_3 is presented. This, in its miniature form, is designed for applications in the field of SHM and NDE of cylindrical structures. The manufacture of the matrix comprised four main steps: deposition of the joint electrode, photolithography, deposition of the second electrode, and lift-off. The characterisation of this matrix has shown that it has a resonance frequency of around 7 MHz. Optical and electrical measurements were carried out on the matrix coupled to an aluminium plate 6 mm thick. The results showed, on the one hand, its sensitivity to Lamb waves for a central excitation frequency of 200 kHz and on the other hand, have demonstrated the quasi-transparent behaviour of the matrix towards these waves. Then, the optical measurements showed the ability of the matrix to detect the Pochhammer-Chree fundamental modes using a piezoceramic transducer as an emitter. Subsequently, two separate semicircular piezoelectric transducers were bound to the cylinder cross section and excited with one phased signal to only generate the F(1,1) mode between 60 kHz and 120 kHz. The μT matrix designed and manufactured is capable of detecting and identifying UGW in a frequency range lower than 1 MHz. These results are promising and pave the way to new NDE inspection techniques using a μT matrix to receive

the data while prioritising the generation of the F(1,1) mode.

In future work, a connected measurements system will be developed in order to adapt the μ T matrix for SHM application. As a first step, a printed circuit board (PCB) can be developed and fixed on the top of the μ Ts matrix. This PCB contains the same number of via-openings as the number of μ Ts and these through holes are distributed with the same pitch as the μ Ts. In the second step, electrical contacts with μ Ts are established by soldering through the board's via-openings. Then, the signals from μ Ts could be directed to an acquisition unit by standard wires or PCB contact paths in a parallel way.

6. Acknowledgements

This research work was funded by the MEAE (Ministère de l'Europe et des Affaires Etrangères), Hauts-de-France Region, France, AUF (Agence Universitaire de la Francophonie), and the Lebanese CNRS.

References

- [1] M. Mitra, S. Gopalakrishnan, Guided wave based structural health monitoring: A review, *Smart Materials and Structures* 25 (2016) 053001.
- [2] E. Le Clézio, M. Castaings, B. Hosten, The interaction of the s0 lamb mode with vertical cracks in an aluminium plate, *Ultrasonics* 40 (2002) 187–192.
- [3] M. J. S. Lowe, O. Diligent, Low-frequency reflection characteristics of the s0 lamb wave from a rectangular notch in a plate, *The Journal of the Acoustical Society of America* 111 (2002) 64–74.
- [4] M. J. S. Lowe, P. Cawley, J.-Y. Kao, O. Diligent, The low frequency reflection characteristics of the fundamental antisymmetric lamb wave a0 from a rectangular notch in a plate, *The Journal of the Acoustical Society of America* 112 (2002) 2612–2622.
- [5] R. Soleimanpour, C.-T. Ng, Scattering of the fundamental anti-symmetric lamb wave at through-thickness notches in isotropic plates, *Journal of Civil Structural Health Monitoring* 6 (2016) 447–459.
- [6] L. Pochhammer, Ueber die fortpflanzungsgeschwindigkeiten kleiner schwingungen in einem unbegrenzten isotropen kreisylinder (1876).
- [7] M. Lowe, D. Alleyne, P. Cawley, Defect detection in pipes using guided waves, *Ultrasonics* 36 (1998) 147–154.
- [8] S. Djili, F. Benmeddour, E. Moulin, J. Assaad, F. boubenider, Notch detection in copper tubes immersed in water by leaky compressional guided waves, *NDT & E International* 54 (2013) 183–188.
- [9] A. Demma, P. Cawley, M. Lowe, A. G. Roosenbrand, The reflection of the fundamental torsional mode from cracks and notches in pipes, *The Journal of the Acoustical Society of America* 114 (2003) 611–625.
- [10] A. Ghavamian, F. Mustapha, B. Baharudin, N. Yidris, Detection, localisation and assessment of defects in pipes using guided wave techniques: A review, *Sensors* 18 (2018) 4470.
- [11] F. Benmeddour, F. Treyssède, L. Laguerre, Numerical modeling of guided wave interaction with non-axisymmetric cracks in elastic cylinders, *International Journal of Solids and Structures* 48 (2011) 764–774.
- [12] E. H. Ling, R. H. Abdul Rahim, A review on ultrasonic guided wave technology, *Australian Journal of Mechanical Engineering* (2017) 1–13.
- [13] X. Zhang, Z. Tang, F. Lü, X. Pan, Excitation of dominant flexural guided waves in elastic hollow cylinders using time delay circular array transducers, *Wave Motion* 62 (2016) 41–54.
- [14] P. S. Lowe, R. M. Sanderson, N. V. Boulgouris, A. G. Haig, W. Balachandran, Inspection of cylindrical structures using the first longitudinal guided wave mode in isolation for higher flaw sensitivity, *IEEE Sensors Journal* 16 (2016) 706–714.
- [15] Y. Qiu, J. Gigliotti, M. Wallace, F. Griggio, C. Demore, S. Cochran, S. Trolrier-McKinstry, Piezoelectric micromachined ultrasound transducer (PMUT) arrays for integrated sensing, actuation and imaging, *Sensors* 15 (2015) 8020–8041.
- [16] W. Zhou, F.-G. Yuan, T. Shi, Guided torsional wave generation of a linear in-plane shear piezoelectric array in metallic pipes, *Ultrasonics* 65 (2016) 69–77.
- [17] S. Quignon, Synthèse et caractérisations de couches minces de matériaux piézoélectriques sans plomb, 2013.
- [18] R. S. Weis, T. K. Gaylord, Lithium niobate: Summary of physical properties and crystal structure, *Applied Physics A Solids and Surfaces* 37 (1985) 191–203.
- [19] J. Cannata, T. Ritter, Wo-Hsing Chen, R. Silverman, K. Shung, Design of efficient, broadband single-element (20–80 MHz) ultrasonic transducers for medical imaging applications, *IEEE Transactions on Ultrasonics, Ferroelectrics and Frequency Control* 50 (2003) 1548–1557.
- [20] Y. Fu, J. Luo, N. Nguyen, A. Walton, A. Flewitt, X. Zu, Y. Li, G. McHale, A. Matthews, E. Iborra, H. Du, W. Milne, Advances in piezoelectric thin films for acoustic biosensors, acoustofluidics and lab-on-chip applications, *Progress in Materials Science* 89 (2017) 31–91.
- [21] S.-E. Hebaz, F. Benmeddour, E. Moulin, J. Assaad, Semi-analytical discontinuous galerkin finite element method for the calculation of dispersion properties of guided waves in plates, *The Journal of the Acoustical Society of America* 143 (2018) 460–469.
- [22] T. Meeker, A. Meitzler, et al., Guided wave propagation in elongated cylinders and plates, *Physical Acoustics-Principles and Methods* (1964) 111–167.